12
Terbium(III) Footprinting as a Probe of RNA Structure and Metal Binding Sites

Dinari A. Harris, Gabrielle C. Todd, and Nils G. Walter

12.1
Introduction

Cations play a pivotal role in RNA structure and function. A functional RNA tertiary structure is stabilized by metal ions that neutralize and, in the case of multivalent ions, bridge the negatively charged phosphoribose backbone [1, 2]. This chapter describes the use of the trivalent lanthanide metal ion terbium(III), abbreviated Tb^{3+} in the following, as a versatile probe of RNA secondary and tertiary structure, as well as an indicator of high-affinity metal ion binding sites. Tb^{3+} was chosen over other lanthanide metals because aqueous Tb^{3+} complexes have a low $pK_a \sim 7.9$, which conveniently generates enough $Tb(OH)(aq)^{2+}$ around neutral pH to hydrolyze the RNA backbone. Cleavage occurs *via* deprotonation of the 2′-hydroxyl group and nucleophilic attack of the resulting oxyanion on the adjacent 3′, 5′-phosphodiester to form 2′, 3′-cyclic phosphate and 5′-hydroxyl termini (Figure 12.1) [3]. In addition, Tb^{3+} has a similar ionic radius (0.92 Å) as Mg^{2+} (0.72 Å) and a similar preference for oxygen and nitrogen ligands over softer ones, while further generating a specific fluorescence signature upon binding to RNA [4–6]. Thus, Tb^{3+} binds to similar sites on RNA as Mg^{2+} but with 2–4 orders of magnitude higher affinity, commensurate with its higher charge density. As a consequence, low (micromolar) concentrations of Tb^{3+} ions readily displace medium (millimolar) concentrations of Mg^{2+} ions from both specific and non-specific high-affinity binding sites and promote slow phosphodiester backbone cleavage, revealing the location of Mg^{2+}-binding sites in the RNA [6]. Higher (millimolar) concentrations of Tb^{3+} ions bind diffusely to RNA and result in backbone cleavage in a sequence-independent manner, preferentially cutting solvent-accessible, single-stranded, or non-Watson-Crick base-paired regions. Incubation with high concentrations of Tb^{3+} provides a footprint of the RNA's secondary and tertiary structure with nucleotide resolution [5–12].

Tb^{3+} can be a very straightforward and useful probe of metal binding and tertiary structure formation in RNA. However, there are several precautions that need to be considered in order to obtain a reliable and reproducible RNA footprinting pattern. As low (micromolar) concentrations of Tb^{3+} bind to high-affinity metal binding

Handbook of RNA Biochemistry, Second Edition.
Edited by R.K. Hartmann, A. Bindereif, A. Schön, and E. Westhof.

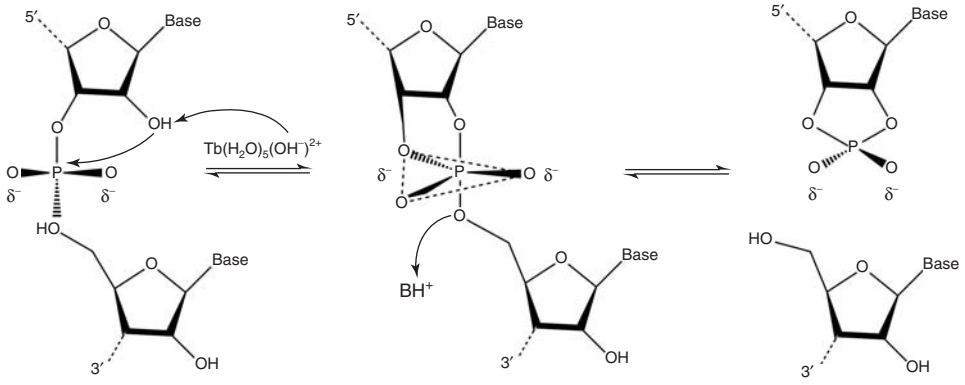

Figure 12.1 Mechanism of RNA backbone cleavage by $Tb(OH)(aq)^{2+}$. Cleavage occurs *via* deprotonation of the 2′-hydroxyl group and nucleophilic attack of the resulting oxyanion on the adjacent 3′, 5′-phosphodiester to form 2′, 3′-cyclic phosphate and 5′-hydroxyl termini.

sites within a folded RNA, while high (millimolar) concentrations produce a footprinting pattern of solvent-accessible regions, it is critical to perform Tb^{3+}-induced cleavage reactions over a wide range of Tb^{3+} concentrations. To ensure conformational homogeneity, prefolding the RNA under optimized buffer conditions and magnesium concentrations is necessary. This is especially important when trying to identify metal binding sites, as there will be relatively few cleavage events at low Tb^{3+} concentrations. All cleavage reactions should be performed near physiological pH (7.0–7.5) to allow for the accumulation of the cleavage-active $Tb(OH)(aq)^{2+}$ species [8]. Insoluble polynuclear hydroxo aggregates of Tb^{3+} can form at pH 7.5 and above [13, 14], which should be avoided. Another parameter that needs to be empirically optimized is the temperature and duration of the metal ion-induced cleavage reaction. Higher temperatures not only result in faster cleavage rates but also increase the amount of background degradation. Therefore, typical reaction temperatures range from 25 to 45 °C over a period of 0.5–2 h. All of these parameters need to be well established before carrying out Tb^{3+} footprinting experiments in earnest.

Tb^{3+} Footprinting of Short RNAs

Materials

Reagents and Buffers

- RNA of interest, end-labeled, and gel-purified
- Appropriate buffers to fold the RNA (usually Tris, MES, and/or HEPES of desired pH)
- 1 M $MgCl_2$ solution
- 100 mM $TbCl_3$ in 5 mM sodium cacodylate buffer, pH 5.5 (store in small aliquots at −20 °C)

- 0.5 M Na_2EDTA, pH 8.0
- 3 M Na(OAc), pH 5.2
- Urea loading buffer: 8 M urea, 50 mM Na_2EDTA , pH 8.0, 0.01% bromophenol blue, 0.01% xylene cyanol.

Equipment

- Heating block at 90 °C
- Water bath
- Phosphor screens and phosphorimager with appropriate software (e.g., Typhoon 9410 Variable Mode Imager with ImageQuant software (GE Healthcare))
- Vacufuge concentrator (Eppendorf).

Protocol 1

1) Before performing Tb^{3+}-mediated footprinting of an RNA molecule, the RNA should be end-labeled (typically with ^{32}P at either the 5′ or 3′ end), purified by denaturing gel electrophoresis, and stored in water (or an appropriate buffer) at −20 °C. For experimental details on ^{32}P-end-labeling and gel purification of RNA, see Chapters 3 and 9.
2) Prepare a single pool with 250 000–500 000 cpm (typically 0.5–2 pmol) of end-labeled RNA per reaction. The total pool volume should be sufficient for single or duplicate reactions at each of the desired Tb^{3+} concentrations. Heat-denature the RNA pool at 90 °C for 2 min under appropriate buffer conditions, but in the absence of divalent metal ions to avoid RNA hydrolysis.
3) Prefold the RNA by incubating the pool at an optimized temperature (typically 25–45 °C) for approximately 10 min to ensure structural homogeneity. Some RNAs fold best when a slow-cooling procedure is used, or when certain cations are already added at this stage.
4) To obtain the desired Mg^{2+} concentration, add an aliquot of $MgCl_2$ from an appropriately diluted stock solution and equilibrate at the optimized temperature for an additional 5–10 min. At this point, the total volume of the RNA pool should be 8 µl per reaction aliquot.
5) From the 100 mM $TbCl_3$ stock solution, make a serial set of $TbCl_3$ dilutions in water, ranging from micromolar to millimolar concentrations (5 × over the final reaction concentration). This wide range of $TbCl_3$ concentrations should be sufficient to probe for both high-affinity metal binding sites and secondary/tertiary structure formation. *Note: The 100 mM $TbCl_3$ stock solution is dissolved in a 5 mM sodium cacodylate buffer at pH 5.5 to prevent formation of terbium(III) hydroxide precipitates at higher pH. The $TbCl_3$ dilutions in water should be made immediately before use. A serial set of dilutions is recommended to ensure consistency in cleavage band intensity between gel lanes. Use a fresh aliquot of 100 mM $TbCl_3$ stock solution each time. Final $TbCl_3$ concentrations used in the cleavage reactions should be optimized together with other experimental conditions for the specific RNA and experimental goal.*

6) To initiate Tb^{3+}-mediated cleavage, mix an 8-µl aliquot from the refolded RNA pool with 2 µl of an appropriate dilution of $TbCl_3$ to achieve the desired final Tb^{3+} concentration (typically ranging from 5 µM to 5 mM, in addition to a 0 mM Tb^{3+} control). Continue to incubate at the optimized temperature for an optimized amount of time (typically 30 min to 2 h). *Note: The incubation times should be chosen to generate a partial digestion pattern of end-labeled RNA under single-hit conditions. Extended incubation times will increase secondary hits that may reflect structural distortions of the RNA due to the preceding cleavage event.*
7) Quench the cleavage reaction by adding EDTA, pH 8.0, to a final concentration of 50 mM (or at least a twofold excess over the total concentration of multivalent metal ions in the reaction aliquot).
8) Perform an ethanol precipitation of the RNA by adding Na(OAc) to a final concentration of 0.3 M and 2–2.5 vol of 100% ethanol and precipitate at −20 °C overnight. Centrifuge 30 min at 12 000 *g*, 4 °C. Decant supernatant, wash with 80% (v/v) ethanol, decant supernatant, and dry RNA in a Speedvac evaporator. Redissolve samples in 10–20 µl of urea loading buffer.
9) Partial alkaline hydrolysis and RNase T1 digestion reactions of refolded RNA from the same pool should be performed as calibration standards by incubating the end-labeled RNA in the appropriate buffers.
10) Heat samples at 90 °C for 5 min and place on ice water to snap cool. Analyze the cleavage products on a high-resolution denaturing (8 M urea) polyacrylamide sequencing gel, using the partial alkaline hydrolysis and RNase T1 digestion reactions as size markers to identify the specific Tb^{3+} hydrolysis products at nucleotide resolution. *Note: In the example cited below, an 8 M urea, 20% polyacrylamide gel was poured between 35 × 45 glass plates with a 1-mm wedged spacer and was run at a constant power of 80 W for separating the cleavage products of a radiolabeled 39-mer RNA. Identical samples can be loaded at different times on the same gel to resolve different regions of longer RNA.*
11) Product bands are directly visualized by exposing a phosphor screen to the gel. *Note: The exposure can take several hours to overnight, depending on the level of radioactivity of the bands in the gel.*
12) Quantify the full-length RNA and cleavage product bands using a volume count method. (For a more qualitative evaluation, a line scan method can be used.) At every Tb^{3+} concentration, calculate a normalized extent of cleavage (χ) by substituting the peak intensities in the equation:

$$\chi = \frac{\left(\dfrac{\text{Band intensity at nucleotide } a_x}{\sum_{i=1}^{n} \text{Band intensity at nucleotide } a_i} \right) \gamma \text{ mM } [Tb^{3+}]}{\left(\dfrac{\text{Band intensity at nucleotide } a_x}{\sum_{i=1}^{n} \text{Band intensity at nucleotide } a_i} \right) 0 \text{ mM } [Tb^{3+}]}$$

where y is the Tb^{3+} concentration in a particular cleavage reaction and x is the analyzed nucleotide position of the RNA. 0 mM [Tb^{3+}] signifies a control reaction incubated in the same manner as the Tb^{3+}-containing ones except that water is added instead of Tb^{3+} solution. A χ value of ≥ 2 indicates significant cleavage over background degradation. *Note: By dividing the ratio of a single-band intensity over total RNA (that is, the sum of all individual bands including the intact RNA) in the presence of Tb^{3+} by the ratio of a single-band intensity over total RNA in the absence of Tb^{3+}, one normalizes for the effect of non-specific background degradation.*

Footprinting Long RNAs by Primer Extension

The protocol in the section "Tb^{3+} Footprinting of Short RNAs" presents a simple and rapid method for determining the secondary structure and metal binding sites of small RNAs. However, when the length of the RNA of interest is greater than ~100 nt, it becomes difficult to resolve all of the footprinting data on a single sequencing gel, even when loading the same sample multiple times while the gel is running. This difficulty can be overcome by the use of primer extension analysis. Multiple primers complementary to different regions of the RNA of interest (~100 nt apart) can be used to obtain footprinting information for the entire length of a long RNA in a single sequencing gel [15, 16].

Although the primer extension method is very powerful, additional steps are necessary to correctly interpret footprinting data. First, dideoxynucleotide (ddNTP) sequencing reactions must be performed with each primer to determine the sequence of the RNA. When these sequencing ladders are resolved on a gel in parallel with primer extension reactions of footprinted RNA, they enable site-specific identification of the nucleotides cleaved by Tb^{3+}. A primer extension reaction on unmodified RNA must also be resolved in parallel, and any signal in this lane must be subtracted from experimental data lanes to account for low processivity or structurally induced stops of the reverse transcriptase during the primer extension assay [15, 16]. Finally, primer extension analysis has the disadvantage that information at the very ends of the RNA of interest is often lost. Structural information at the 5′ end of the RNA can be masked by the heavy signal from the full-length product generated by the necessary single-hit footprinting conditions. Information at the 3′ end of the RNA of interest cannot be obtained because the 3′-terminal 20–30 nt are masked by the primer. These problems can sometimes be overcome by adding spacer sequences to the 5′ and 3′ ends of the RNA [15], although additional experiments should be done to ensure that these regions do not alter the structure and function of the RNA of interest.

Materials

Reagents and Buffers

- RNA of interest, unlabeled, and gel-purified
- 0.5 × TE, pH 8.0 (5 mM Tris-HCl, 0.5 mM EDTA)

- SuperScript III Reverse Transcriptase and included 5× First-Strand Buffer (Life Technologies Invitrogen)
- DNA primer(s) (Life Technologies Invitrogen), 5′-end-labeled with ^{32}P
- 10 mM Deoxynucleotides (dNTPs) (GE Healthcare Life Sciences)
- ddNTP Set, 5 mM Solutions (ddATP, ddCTP, ddGTP, ddTTP) (GE Healthcare Life Sciences)
- 100 mM DTT.

Equipment

- Heating block at 90 °C
- Water bath
- Phosphor screens and phosphorimager with appropriate software (e.g., Typhoon 9410 Variable Mode Imager with ImageQuant software (GE Healthcare)).

Protocol 2

1) Design DNA oligomers that are complementary to the RNA of interest, 3′ of the region to be probed. DNA oligomers should be 20–30 nt in length, with a melting temperature between 55 and 60 °C. *Note: Primers should be spaced ~100 nt apart along the RNA of interest to obtain reliable structural data for the entire molecule.*
2) Label the 5′ end of primers with ^{32}P and gel-purify. Redissolve primers in water and store at −20 °C.
3) Refold unlabeled RNA of interest as described in Protocol 1, steps 2–4. Refold a pool of RNA (0.5–2 pmol RNA in 8 µl per reaction) accounting for the number of primers, number of Tb^{3+} concentrations to be tested, negative controls, and sequencing lanes (discussed below). The same pool of refolded RNA should be used for all reactions and controls.
4) Perform Tb^{3+} footprinting as described in Protocol 1, steps 5–7, but scale up each footprinting reaction by the number of primers needed to probe the entire RNA.
5) A negative control (0 mM Tb^{3+}), where water instead of a Tb^{3+} solution is added to the RNA, should be performed in parallel for each primer. This reaction should be scaled up such that there is enough RNA to generate a dideoxy sequencing ladder as well. *Note: A negative control is necessary as non-footprinted RNA will reveal natural stops in the primer extension reaction because of idiosyncrasies of the reverse transcriptase or stable secondary structures in the RNA.*
6) Precipitate footprinted RNAs as in Protocol 1, step 8, but redissolve pellets in 10 µl of 0.5 x TE buffer, pH 8.0, per primer extension reaction for probed and unprobed RNA. For dideoxy sequencing reactions, redissolve in only 9 µl of 0.5 x TE buffer, pH 8.0.
7) Anneal 3 µl of ^{32}P-end-labeled primer (150 000 cpm, or more for long RNAs) per 10 µl aliquot of footprinted RNA by heating to 65 °C for 5 min, incubating at 45 °C for 2 min, and then cooling on ice.

8) Prewarm RNA:primer complex and reverse transcriptase mix (4 µl 5× First-Strand buffer, 1 µl 100 mM DTT, 1 µl 10 mM each dNTP, and 1 µl Superscript III reverse transcriptase) separately for 10 s at 45 °C. Transfer 7 µl of reverse transcriptase mix to the RNA:primer complex and incubate tubes at 52 °C for 5 min to extend primers. Place reactions at 65 °C for 5 min to inactivate the reverse transcriptase and return reactions to ice.
9) Perform dideoxy sequencing reactions as just described in steps 7 and 8, except for the addition of 1 µl of an individual ddNTP solution at a concentration empirically optimized to produce a banding pattern, before addition of the reverse transcriptase mix.
10) Precipitate reactions as described in Protocol 1, step 8, and analyze reactions by denaturing PAGE as described in Protocol 1, steps 10–12.

12.2 Application Example

Tb^{3+} has been successfully used on a number of RNAs as a probe for high-affinity metal binding site localization and tertiary structure determination. For example, taking advantage of its luminescent and RNA footprinting properties, Tb^{3+} has revealed subtle structural differences between the precursor and product forms of the hepatitis delta virus (HDV) ribozyme [5, 6]. The HDV ribozyme is a unique RNA motif found in the human HDV, a satellite of the hepatitis B virus that leads to frequent progression toward liver cirrhosis in millions of patients worldwide [17]. There is a strong interest, both for scientific and medical reasons, in understanding the structure–function relationship of this catalytic RNA. We found that the Tb^{3+}-mediated footprinting pattern of the 3′ product (3′P) complex of a *trans*-acting version of the HDV ribozyme (Figure 12.2a), obtained in the presence of millimolar Tb^{3+} concentrations, is consistent with a post-cleavage crystal structure. In particular, protection is observed in all five helical stems, P1 through P4 and P1.1, while the backbone of the L3 loop region and that of the J4/2 joining segment are strongly cut (Figure 12.2) [5]. Cuts in J4/2 are particularly relevant, as it encompasses the catalytic residue C75 and its neighboring G76, and the strong Tb^{3+} hits implicate it as a region of high negative charge density with high affinity for metal ions.

Strikingly, Tb^{3+} footprinting reveals the precursor (ncS3) structure as distinct; while P1, P2, P3, and P4 remain protected, both the 5′ and 3′ segments of the P1.1 stem (as well as U20, immediately upstream) are strongly hydrolyzed, suggesting that this helix in the catalytic core is formed to a lesser extent than in the product complex. In addition, scission in J4/2 extends to A77 and A78, implying that the ribose zipper motif involving these nucleotides may not be fully formed in the precursor complex (Figure 12.2b). These differences in the extent of backbone scission in the precursor *versus* the 3′ product complexes show that a significant conformational change occurs upon HDV ribozyme catalysis and 5′ product dissociation from the 3′ product [5, 6, 11, 12].

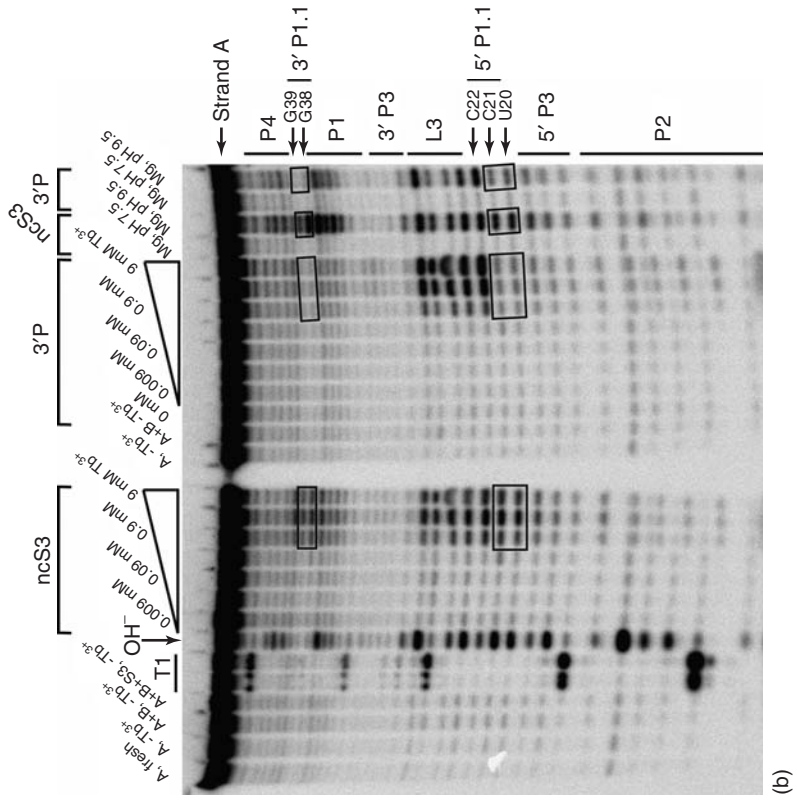
Strand A
P4
G39
G38
3′ P1.1
P1
3′ P3
L3
C22
C21
U20
5′ P1.1
5′ P3
P2
A, fresh
A, -Tb3+
A+B, -Tb3+
A+B+S3, -Tb3+
T1
OH−
ncS3
0.009 mM
0.09 mM
0.9 mM
9 mM Tb3+
3′P
A, -Tb3+
A+B -Tb3+
0 mM
0.009 mM
0.09 mM
0.9 mM
9 mM Tb3+
ncS3
3′P
Mg, pH 7.5
Mg, pH 9.5
Mg, pH 7.5
Mg, pH 9.5
(b)
S3
3′P
Strand A
Strand B
P1
P1.1
P2
P3
P4
J4/2
(a)

Figure 12.2 Tb^{3+} footprinting of the *trans*-acting HDV ribozyme. (a) Synthetic HDV ribozyme construct D1. The ribozyme portion is composed of two separate RNA strands A and B. The 3′ product (3′P) strand, shown in gray letters, interacts with the ribozyme by forming helix P1. The substrate variant S3 contains eight additional nucleotides (gray) 5′ of the cleavage site (arrow). To generate non-cleavable substrate analogs, the 2′-OH of the underlined nucleotide immediately 5′ of the cleavage site was modified to 2′-methoxy and the suffix ''nc'' added to their name (Figure 12.3). Dashed lines represent tertiary structure hydrogen bonds of C75 and the ribose zipper of A77 and A78 in J4/2. Note that although HDV ribozyme construct D1 lacks the U27 present in other HDV ribozyme variants, the canonical numbering of the HDV ribozyme is maintained here for better comparability. (b) Tb^{3+}- and Mg^{2+}-mediated footprint of the (5′-^{32}P)-labeled HDV ribozyme strand A upon incubation with Tb^{3+} for 2 h in 40 mM Tris-HCl, pH 7.5, 11 mM $MgCl_2$ at 25 °C. From left to right as indicated: Strand A fresh after radiolabeling; incubated in buffer without Tb^{3+}; incubated with excess strand B in buffer without Tb^{3+}; incubated with excess strand B and non-cleavable substrate analog ncS3 in buffer without Tb^{3+}; RNase T1 digest; alkali (OH^-) ladder; footprint of strand A with increasing Tb^{3+} concentrations in the presence of excess strand B and ncS3; strand A incubated in buffer without Tb^{3+}; incubated with excess strand B in buffer without Tb^{3+}; footprint with increasing Tb^{3+} concentrations in the presence of excess strand B and 3′ product (3′P). As the Tb^{3+} concentration increases, backbone scission becomes more intense. The 5′ and 3′ segments of P1.1 (boxed) footprint very differently in the precursor and product complexes. Last four lanes on the right: Mg^{2+}-induced cleavage at pH 9.5 and 37 °C; from left to right: precursor (ncS3) complex, control incubated at pH 7.5; precursor complex, footprinted at pH 9.5; product complex, control incubated at pH 7.5; product complex, footprinted at pH 9.5. (Reprinted with permission from Ref. [5].)

While previous evidence from fluorescence resonance energy transfer (FRET) [18], 2-aminopurine fluorescence quenching [19], and NMR spectroscopy [20, 21] had already hinted at structural differences between the precursor and 3′ product forms of the *trans*-acting HDV ribozyme, Tb^{3+}-mediated footprinting complements these techniques by providing specifics of these rearrangements at nucleotide resolution. Particularly intriguing are the differences in the catalytic core structure around C75 and P1.1 that may control access to the cleavage transition state and may therefore explain differences in the catalytic rate constants for substrates with different 5′ sequences (Figure 12.3) [5, 12]. In fact, the 5′ substrate sequence subtly modulates the Tb^{3+} hydrolysis pattern, but all the substrates consistently show strong cuts in the P1.1 stem and the ribose zipper motif in J4/2 (Figure 12.3). This implies that in the precursor, these tertiary structure interactions are not fully formed, in contrast to the 3′P complex. Interestingly, these subtle differences in the catalytic core structure of the various precursor complexes translate into significant changes in FRET efficiency between fluorophores attached to the termini of P4 and P2 [5]. Taken together, these results indicate that the various precursor complexes differ in structure both locally (in the catalytic core) and globally (as measured by FRET), providing an explanation for the wide range of catalytic activities of substrates with varying 5′ extensions [5, 12, 22].

Several other laboratories have also found Tb^{3+} to be a useful probe of high-affinity metal binding sites and RNA tertiary structure. Musier-Forsyth and

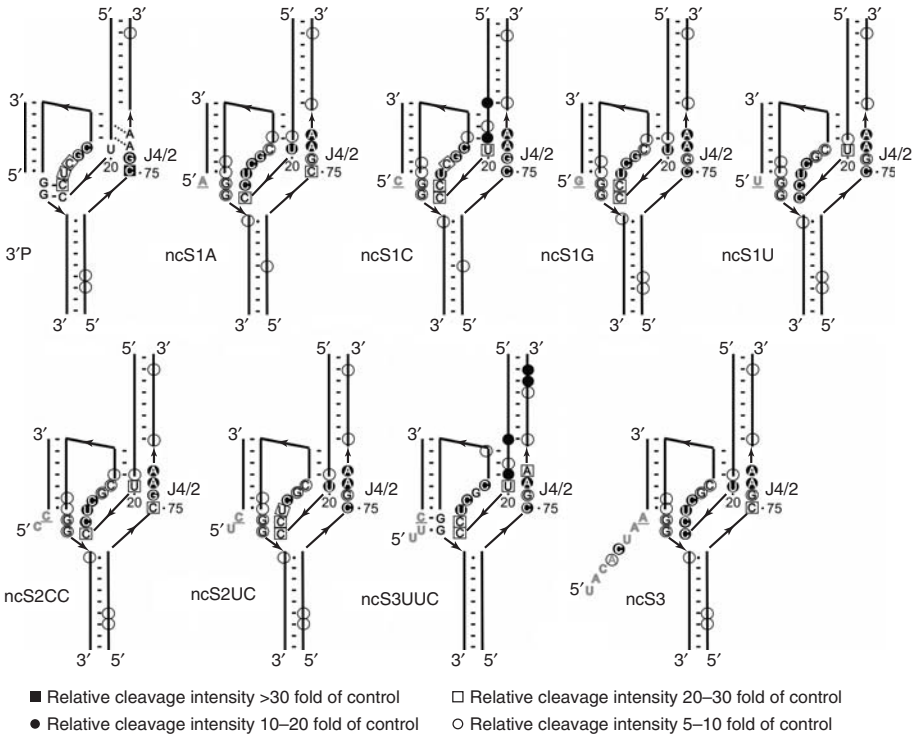

Figure 12.3 Sites of backbone scission mediated by 3 mM Tb^{3+} in 40 mM Tris-HCl, pH 7.5, 11 mM $MgCl_2$ at 25 °C and superimposed onto 2D representations of the precursor and product HDV ribozyme secondary structures. Only the catalytic core residues are explicitly shown. Relative scission intensities were calculated as described in Protocol 1 and are represented by the symbol code. Scissions are located 3′ of the indicated nucleotides. Only the product structure (3′P) is likely to fully form P1.1 and the ribose zipper of A77 and A78 in J4/2; consequently, dashes indicating the base pairs in P1.1 and dashed lines illustrating the ribose zipper interactions are solely shown for the structure of the 3′P complex. (Reprinted with permission from Ref. [5].)

coworkers were able to show that Tb^{3+} substitutes for several well-known metal binding sites in human $tRNA^{Lys,3}$ and works as a sensitive probe of tertiary structure. At low Tb^{3+} concentrations, cleavage of $tRNA^{Lys,3}$ is restricted to nucleotides that were previously identified by X-ray crystallography as specific metal binding pockets [7]. The use of higher Tb^{3+} concentrations resulted in an overall footprint of the L-shaped tRNA structure, showing increased cleavage in the loop regions (D and anticodon loop). HIV nucleocapsid protein could then be shown to disrupt the tRNA's metal binding pockets and, at higher concentrations, to destabilize the tRNA acceptor-TψC stem domain, as inferred from increased Tb^{3+} cleavage in this region of the tRNA [9]. Other RNAs that have similarly been studied by Tb^{3+}-mediated footprinting include the hammerhead ribozyme [4], an aminoacyl-transferase ribozyme [23, 24], RNase P [25], and group II intron ribozymes [26].

12.3 Troubleshooting

Initial titration experiments will be necessary to obtain the optimal Tb^{3+} concentration(s) to be used for structure probing of any individual RNA (typical Tb^{3+} and RNA concentrations for determining tertiary structural features are ~1–5 mM and 1 μM, respectively). The trivalent Tb^{3+} has been shown to induce slight perturbations of RNA structure [7], but careful titration will reveal the optimal Tb^{3+}:RNA ratio needed for detecting unbiased secondary and tertiary structure features in a given RNA molecule.

To verify a high-affinity metal ion binding site, it is advisable to first decrease the Tb^{3+} concentration until a very limited cleavage pattern is observed (typically at 10–100 μM Tb^{3+}), and then to perform a competition experiment with increasing concentrations of Mg^{2+}. The intensity (or fraction of RNA cleaved at a particular nucleotide position) should decrease as the Mg^{2+} concentration increases. Quantifying the intensities of cleaved bands at each nucleotide position directly relates to the structure of RNA. It is critical to keep the extent of total cleavage lower than 20% of the uncleaved or full-length band to ensure that each RNA molecule is (at most) undergoing a single cleavage event. Finally, it is important to keep in mind that Tb^{3+} footprinting may not reveal all of the high-affinity metal ion binding sites. This complication may occur when there is steric hindrance preventing Tb^{3+} from binding close to the 2′-hydroxyl group on the ribose. For example, A-type RNA helices have an unfavorable geometry for Tb^{3+} binding, and therefore, strong metal ion binding sites that occur in RNA helical regions may be underestimated or remain undetected when using Tb^{3+} as probe [26].

12.4 Frontiers in Footprinting Data Analysis

A recent development in the field of RNA structure probing is the advent of a high-throughput method for the analysis of primer extension reactions by capillary electrophoresis (CE). This method, pioneered by Kevin Weeks and coworkers [27], bypasses the time-consuming steps of working with radioactivity and running sequencing gels and automates much of the data analysis. Primer extension reactions are carried out with 5′-fluorescently labeled DNA primers, and the cDNA fragments are resolved using a multichannel CE DNA sequencer [27]. The software package ShapeFinder [28] converts output electropherograms of peak intensity *versus* time into nucleotide reactivity *versus* location of that nucleotide. Data conversion subtracts background stops in unmodified RNA and aligns the data to sequencing reactions to determine the identity of reactive nucleotides. This method provides a rapid way to analyze many primer extension reactions simultaneously, and fewer overall primers are needed to sequence a long RNA because 300–600 nt can typically be resolved from a single primer [27, 29]. Any type of footprinting, including Tb^{3+} probing, that generates stops during primer

extension can be analyzed by this method, thus making it a very versatile and rapid way to study structure–function relationships in RNA.

References

1. Pyle, A.M. (2002) Metal ions in the structure and function of RNA. *J. Biol. Inorg. Chem.*, **7**, 679–690.
2. Draper, D.E., Grilley, D., and Soto, A.M. (2005) Ions and RNA folding. *Annu. Rev. Biophys. Biomol. Struct.*, **34**, 221–243.
3. Ciesiolka, J., Marciniec, T., and Krzyzosiak, W. (1989) Probing the environment of lanthanide binding sites in yeast tRNA(Phe) by specific metal-ion-promoted cleavages. *Eur. J. Biochem.*, **182**, 445–450.
4. Feig, A.L., Panek, M., Horrocks, W.D. Jr., and Uhlenbeck, O.C. (1999) Probing the binding of Tb(III) and Eu(III) to the hammerhead ribozyme using luminescence spectroscopy. *Chem. Biol.*, **6**, 801–810.
5. Jeong, S., Sefcikova, J., Tinsley, R.A., Rueda, D., and Walter, N.G. (2003) *Trans*-acting hepatitis delta virus ribozyme: catalytic core and global structure are dependent on the 5′ substrate sequence. *Biochemistry*, **42**, 7727–7740.
6. Harris, D.A., Tinsley, R.A., and Walter, N.G. (2004) Terbium-mediated footprinting probes a catalytic conformational switch in the antigenomic hepatitis delta virus ribozyme. *J. Mol. Biol.*, **341**, 389–403.
7. Hargittai, M.R. and Musier-Forsyth, K. (2000) Use of terbium as a probe of tRNA tertiary structure and folding. *RNA*, **6**, 1672–1680.
8. Walter, N.G., Yang, N., and Burke, J.M. (2000) Probing non-selective cation binding in the hairpin ribozyme with Tb(III). *J. Mol. Biol.*, **298**, 539–555.
9. Hargittai, M.R., Mangla, A.T., Gorelick, R.J., and Musier-Forsyth, K. (2001) HIV-1 nucleocapsid protein zinc finger structures induce tRNA(Lys,3) structural changes but are not critical for primer/template annealing. *J. Mol. Biol.*, **312**, 985–997.
10. Harris, D.A. and Walter, N.G. (2003) Probing RNA structure and metal-binding sites using terbium(III) footprinting. *Curr. Protoc. Nucleic Acid Chem.*, **6.8**, 6.8.1–6.8.8.
11. Sefcikova, J., Krasovska, M.V., Spackova, N., Sponer, J., and Walter, N.G. (2007) Impact of an extruded nucleotide on cleavage activity and dynamic catalytic core conformation of the hepatitis delta virus ribozyme. *Biopolymers*, **85**, 392–406.
12. Sefcikova, J., Krasovska, M.V., Sponer, J., and Walter, N.G. (2007) The genomic HDV ribozyme utilizes a previously unnoticed U-turn motif to accomplish fast site-specific catalysis. *Nucleic Acids Res.*, **35**, 1933–1946.
13. Baes, C.F. and Mesmer, R.E. (1976) *The Hydrolysis of Cations*, Wiley Interscience, New York.
14. Matsumura, K. and Komiyama, M. (1997) Enormously fast RNA hydrolysis by lanthanide(III) ions under physiological conditions: eminent candidates for novel tools of biotechnology. *J. Biochem.*, **122**, 387–394.
15. Wilkinson, K.A., Merino, E.J., and Weeks, K.M. (2006) Selective 2′-hydroxyl acylation analyzed by primer extension (SHAPE): quantitative RNA structure analysis at single nucleotide resolution. *Nat. Protoc.*, **1**, 1610–1616.
16. Tijerina, P., Mohr, S., and Russell, R. (2007) DMS footprinting of structured RNAs and RNA-protein complexes. *Nat. Protoc.*, **2**, 2608–2623.
17. Hadziyannis, S.J. (1997) Review: hepatitis delta. *J. Gastroenterol. Hepatol.*, **12**, 289–298.
18. Pereira, M.J., Harris, D.A., Rueda, D., and Walter, N.G. (2002) Reaction pathway of the *trans*-acting hepatitis delta virus ribozyme: a conformational change accompanies catalysis. *Biochemistry*, **41**, 730–740.

19. Harris, D.A., Rueda, D., and Walter, N.G. (2002) Local conformational changes in the catalytic core of the *trans*-acting hepatitis delta virus ribozyme accompany catalysis. *Biochemistry*, **41**, 12051–12061.
20. Luptak, A., Ferre-D'Amare, A.R., Zhou, K., Zilm, K.W., and Doudna, J.A. (2001) Direct pK(a) measurement of the active-site cytosine in a genomic hepatitis delta virus ribozyme. *J. Am. Chem. Soc.*, **123**, 8447–8452.
21. Tanaka, Y., Tagaya, M., Hori, T., Sakamoto, T., Kurihara, Y., Katahira, M., and Uesugi, S. (2002) Cleavage reaction of HDV ribozymes in the presence of Mg^{2+} is accompanied by a conformational change. *Genes Cells*, **7**, 567–579.
22. Shih, I. and Been, M.D. (2001) Energetic contribution of non-essential 5′ sequence to catalysis in a hepatitis delta virus ribozyme. *EMBO J.*, **20**, 4884–4891.
23. Flynn-Charlebois, A., Lee, N., and Suga, H. (2001) A single metal ion plays structural and chemical roles in an aminoacyl-transferase ribozyme. *Biochemistry*, **40**, 13623–13632.
24. Vaidya, A. and Suga, H. (2001) Diverse roles of metal ions in acyl-transferase ribozymes. *Biochemistry*, **40**, 7200–7210.
25. Kaye, N.M., Zahler, N.H., Christian, E.L., and Harris, M.E. (2002) Conservation of helical structure contributes to functional metal ion interactions in the catalytic domain of ribonuclease P RNA. *J. Mol. Biol.*, **324**, 429–442.
26. Sigel, R.K., Vaidya, A., and Pyle, A.M. (2000) Metal ion binding sites in a group II intron core. *Nat. Struct. Biol.*, **7**, 1111–1116.
27. Wilkinson, K.A., Gorelick, R.J., Vasa, S.M., Guex, N., Rein, A., Mathews, D.H., Giddings, M.C., and Weeks, K.M. (2008) High-throughput SHAPE analysis reveals structures in HIV-1 genomic RNA strongly conserved across distinct biological states. *PLoS Biol.*, **6**, e96.
28. Vasa, S.M., Guex, N., Wilkinson, K.A., Weeks, K.M., and Giddings, M.C. (2008) ShapeFinder: a software system for high-throughput quantitative analysis of nucleic acid reactivity information resolved by capillary electrophoresis. *RNA*, **14**, 1979–1990.
29. Watts, J.M., Dang, K.K., Gorelick, R.J., Leonard, C.W., Bess, J.W. Jr., Swanstrom, R., Burch, C.L., and Weeks, K.M. (2009) Architecture and secondary structure of an entire HIV-1 RNA genome. *Nature*, **460**, 711–716.